A surface energy analysis of bioadhesion*

D. H. Kaelble
Science Center, Rockwell International, Thousand Oaks, Ca 91360, USA
and Jovan Moacanin
Jet Propulsion Laboratory, California Institute of Technology, California, USA
(Received 20 October 1976; revised 14 December 1976)

This report applies recently developed surface energy and fracture mechanics relations to the analysis of bioadhesion and biocompatibility. The dispersion α and polar β components of 190 biological and implant surfaces are analysed. The surface energetics relations between bioadhesion and biocompatibility point out that a strongly adsorbed plasma protein film on the implant surface provides the best blood compatibility and low thrombogenic effects. The surface energy relations provide means of selecting optimum implant surface properties and mapping on surface energy diagrams the three phase interactions which define bioadhesion.

INTRODUCTION

A number of literature reports document the general progress in development of biomaterials and surface treatments designed for application in cardiovascular devices[1-8]. The interfacial interaction of biopolymers with blood remains as one of the central problems in establishing biocompatibility of cardiovascular devices[8]. The exposure of blood to a foreign surface produces a complex set of concurrent and sequential events which appear to correlate with the dispersion (London-*d*) and polar (Keesom-*p*) components of surface tension for the implant material. Baier and coworkers[1-7] have reported detailed studies of contact angle measurements of well characterized liquids on biopolymer surfaces. These measurements and surface energetics analysis follow the methodology and definitions of critical surface tension γ_c for wetting of a solid substrate developed by Zisman and coworkers[9].

More recently, Nyilas and coworkers[10], have demonstrated that the wettability data of Baier and coworkers can be utilized in defining the dispersion and polar components of solid surface tension for candidate implant surfaces. This report of Nyilas and coworkers also describes new semiquantitative relations between blood flow, implant surface energetics, and thrombosis. The analysis utilized by Nyilas and coworkers to isolate the dispersion and polar properties of implant surfaces follows definitions and calculations developed and extensively applied by Kaelble and coworkers[11-13]. The surface energetics analysis of Kaelble and coworkers has recently been extended[14] to define the relations between surface energetics and the Griffith fracture mechanics criteria for spontaneous interface bonding and debonding under consitions of combined liquid immersion and added mechanical stress.

This paper discusses the results of applying the new surface energetics criterion of bonding and debonding for improving the quantitative definition of bioadhesion and to clarify the relationship between bioadhesion and biocompatibility. These new surface energy relations now permit mapping the zones of bonding, termed wettability envelopes on surface energy diagrams of dispersion α *versus* polar β components of surface energy. These surface energy α *versus* β diagrams permit graphic presentation of the surface properties and zones of bonding and debonding for the three phases which constitute the interfacial boundary in the biocompatibility analysis.

* Presented at the First Cleveland Symposium on Macromolecules, Structure and Properties of Biopolymers, Case Western Reserve University, Cleveland, Ohio, USA, October 1976.

SURFACE ENERGY ANALYSIS

The general concept for regular adsorption bonding of interfaces utilized in this discussion is summarized in the following relation for interfacial tension[12]:

$$\gamma_{ij} = (\alpha_i - \alpha_j)^2 + (\beta_i - \beta_j)^2 + \Delta_{ij} \quad (1)$$

where the parameters are defined in *Table 1* and subscripts denote interactions from phase *i* and *j*. Interfaces dominated by Van der Waal's interactions are termed regular interfaces

Table 1 Surface energetics relations

$\gamma_{LV} = \gamma_{LV}^d + \gamma_{LV}^p = \alpha_L^2 + \beta_L^2$	(a)
$\gamma_{SV} = \gamma_{SV}^d + \gamma_{SV}^p = \alpha_S^2 + \beta_S^2$	(b)
$W_a = \gamma_{LV}(1 + \cos\theta) \leqslant 2\gamma_{LV}$	(c)
$W_a = 2[\alpha_L\alpha_S + \beta_L\beta_S]$	(d)
$\frac{W_a}{2\alpha_L} = \alpha_S + \beta_S(\beta_L/\alpha_L)$	(e)
$\frac{W_a}{2\alpha_S} = \alpha_L + \beta_L(\beta_S/\alpha_S)$	(f)

where: γ_{LV} = liquid–vapour tension; γ_{SV} = solid–vapour surface tension; α_L,β_L = square root of the respective (London) dispersion γ_{LV}^d and (Keesom) polar γ_{LV}^p parts of γ_{LV}; α_S,β_S = square roots of respective dispersion γ_{SV}^d and polar γ_{SV}^p; W_a = nominal work of adhesion; θ = liquid–solid contact angle

Table 2 Fracture mechanics relations

$$\sigma_c = \left(\frac{2E\gamma_G}{\pi c}\right)^{1/2} = \left(\frac{2E}{\pi C}\right)^{1/2} (R^2 - R_0^2)^{1/2} \geq 0 \quad \text{(a)}$$

$$\gamma_G = R^2 - R_0^2 \quad \text{(b)}$$

$$R_0^2 = 0.25\,[(\alpha_1 - \alpha_3)^2 + (\beta_1 - \beta_3)^2] \quad \text{(c)}$$

$$R^2 = (\alpha_2 - H)^2 + (\beta_1 - K)^2 \quad \text{(d)}$$

$$H = 0.5\,(\alpha_1 + \alpha_3) \quad \text{(e)}$$

$$K = 0.5\,(\beta_1 + \beta_3) \quad \text{(f)}$$

where σ_c = critical crack propagation stress; γ_G = Griffith surface energy for fracture; E = Young's modulus; c = crack length; α_1, β_1 = surface properties of adhesive (ink) phase 1; α_2, α_2 = surface properties of environment phase 2; α_3, β_3 = surface properties of adherend phase 3

and the values of the excess term Δ_{ij} of equation (1) which describes interdiffusion or ionic–covalent interactions can be considered negligible. This is a much more general case than one might expect and permits application of surface energy analysis to a wide range of materials. When $\Delta_{ij} = 0$, equation (1) defines an ideal interface with $\gamma_{ij} = o$ as the special case where $\alpha_i = \alpha_j$ and $\beta_i = \beta_j$.

The special combination of surface energy and fracture mechanics parameters which enter the modified Griffith relation are defined in *Table 2* and show that the Griffith fracture energy γ_G is defined by the following relation:

$$\gamma_G = -\frac{S_2}{2} = R^2 - R_0^2 \quad (2)$$

A circular parabola in $\gamma_G, \alpha_2, \beta_2$ Cartesian space is defined by equation (2). The surface energies α_2 and β_2 for the immersion phase 2 which provide the condition $R < R_0$ provides that the spreading coefficient S_2 for phase 2 is positive with $S_2 > 0$. The predicted consequence for $S_2 > 0$ is that phase 2 should spontaneously debond phase 1 from phase 3 in the absence of rheological restraints. When $R < R_0$ the Griffith fracture energy becomes positive and a critical mechanical stress σ_c which depends on γ_G (see *Table 2*) is now required for crack extension.

The relations of *Table 1* and *Table 2* form the basis for designed experiments which isolate the discrete mechanisms of polar and dispersion interactions across interface. The test liquids of *Table 3* display a wide range of polar character in surface tension with $\beta_l/\alpha_l = 1.53$ for water to $\beta_l/\alpha_l = 0$ for linear hydrocarbons. Inspection of equation (e) in *Table 1* shows that using measured values of work of adhesion W_a by contact angle measurements for liquids of known α_l and β_l permits isolation of the solid–vapour surface properties α_s and β_s. The intercept of the plot of $W_a/2\alpha_l$ *versus* β_l/α_l isolates α_s as the intercept and β_s as the slope. An alternative method of computerized determinant solutions of equation (d) (*Table 1*) has been described and extensively applied which solve for averaged values of γ_{sv}^d, γ_{sv}^p and γ_{sv} their respective standard deviations $\pm\,\delta^d$, δ^p, and δ from mean values[11,12].

In this study contact angle data where $\theta > 0$ and $W_a < 2\gamma_{lv}$ published by Baier and coworkers[1–7] is combined with the liquid surface tension data of *Table 3* in the computerized determinant calculations for γ_{sv}^d, γ_{sv}^p, γ_{sv} and $\pm\,\delta^d$, δ^p, and δ. The surface energetics of 190 biological and implant surfaces were analysed and the results summarized as values of $\alpha_s = (\gamma_{sv}^d)^{1/2}$ and $\beta_s = (\gamma_{sv}^p)^{1/2}$ and the percent standard deviation ($\delta \times 100/\gamma_{sv}$) of γ_{sv} in *Table 4*. The surface number sequence of *Table 4* correlates with the appearance of the original experimental data in the referenced literature to facilitate ease of cross reference. The reference articles and reports cover an important six year period of biomaterials development and testing from 1970 through 1975.

Surfaces no. 1 and no. 2 of *Table 4* represent important biological surfaces and the illustrative results of the surface energy analysis are graphed in *Figure 1*. *Figure 1b* shows the wettability data for human fibrinogen thin film as defined by equation (e) of *Table 1*. The solid linear curve of *Figure 1b* graphs the computer calculated average values $\gamma_{sv}^d = 24.6$ and $\gamma_{sv}^p = 13.5$ dyne/cm while the broken curves define the standard deviation $\delta^d = \pm 0.7$ and $\delta^b = \pm 0.9$ dyne/cm. As shown in *Figure 1b* the experimental values of $W_a/2\alpha_l$ form a reasonably linear curve which conforms well with the theory of *Table 1* and the computer solutions.

The data points and linear curves of *Figure 1a* show the larger uncertainty in α_s and β_s values for vein intimal surface no. 2 of *Table 4*. Referring to the discussion of Baier *et al.*[1] it is evident that this surface is soft and deformable, the experiment complicated, additionally possible interdiffusion modifies the contact angle data for water and glycerol. As shown in *Figure 1a*, this analysis permits isolation of a low dispersion and high polar surface energy for the vein intimal surface. Considering the highly hydrated state of the vein intimal surface, it is to be expected that the vein surface properties $\alpha = 4.42$ (dyne/cm)$^{1/2}$ and $\beta = 6.18$ (dyne/cm)$^{1/2}$ are closely similar to the surface tension properties of water where $\alpha = 4.67$ (dyne/cm)$^{1/2}$ and $\beta = 7.14$ (dyne/cm)$^{1/2}$.

Available literature references[14,15] describe the surface tension of blood plasma as equivalent to saline solution with surface tension γ_{lv} = 72 to 74 dyne/cm, which is essentially equivalent to pure water with $\gamma_{lv} = 72.8$ dyne/cm. Further studies may show that surfactant effects of blood plasma constituents can produce variable values of β_l with nearly constant α_l in which $\beta_l = 7.14$ (dyne/cm)$^{1/2}$ represents a maximum value. This result has been described by Kaelble[16] for aqueous detergent solutions above the critical micelle concentration. For this discussion, the surface properties of pure water with $\alpha_l = 4.67$ and $\beta_l = 7.14$ (dyne/cm)$^{1/2}$ are

Table 3 Surface tension properties of test liquids at 20°C

Test liquid	γ_{lv} (dyne/cm)	α_l	β_l	Reference
Water	72.8	4.67	7.14	10, 13
Glycerol	63.4	6.10	5.12	10
Formamide	58.2	6.28	4.32	10
Dithioglycol	54.0	6.20	3.94	10
Methylene iodide	50.8	6.83	2.05	10
Ethylene glycol	48.3	5.41	4.36	13
S-Tetrabromoethane	47.5	6.49	2.32	10
α-Bromonaphthalene	44.6	6.68	3.59	10
Tricresyl phosphate	40.9	6.26	1.30	13
1-Methylnaphthalene	38.7	5.04	3.65	10
Dicyclohexyl	33.0	5.74	0	10
n-Hexadecane	27.6	5.24	0	13
n-Tetradecane	26.7	5.17	0	10
n-Tridecane	25.9	5.09	0	10
n-Dodecane	25.4	5.04	0	10
n-Decane	23.9	4.89	0	10
n-Nonane	22.8	4.77	0	10
n-Octane	21.8	4.67	0	10
n-Heptane	20.3	4.51	0	10

Table 4 Dispersion (α) and polar (β) surface energy properties of biological and implant materials

Reference	Surface no. 4	Surface	α $(\text{dyne/cm})^{1/2}$	β $(\text{dyne/cm})^{1/2}$	$\frac{100\delta}{\gamma_{sv}}$
1	1	Human fibrinogen thin film	4.96	3.67	1.17
1	2	Vein intimal surface, dog, air–liquid interface	4.42	6.18	13.00
1	3	Stellite plate–normal polish–distilled water rinse (a)	4.87	1.40	2.94
1	4	Same after vigorous detergent wash (b)	5.01	1.55	2.33
1	5	Stellite cage of Starr–Edwards valve after vigorous detergent wash (c)	5.08	2.90	1.60
1	6	Stellite 21 ring normal polish (d)	5.21	1.62	2.95
1	7	Same after implantation and after vigorous detergent wash (e)	4.99	5.09	5.03
1	8	Stellite 21 ring poorly organic coated (f)	5.08	1.73	2.66
1	9	Same after implantation and adsorption of protein (g)	5.03	4.73	5.74
1	10	Same after vigorous detergent wash (h)	4.53	6.87	11.99
1	11	Stellite 21 ring only partly organic coated (i)	5.75	2.95	2.65
1	12	Same after implantation and adsorption of protein (j)	5.02	4.38	4.35
1	13	Same after vigorous detergent wash (k)	4.54	6.83	13.14
2	14	Thromboresistant TDMAC heparinized silicone – before implantation	5.92	4.09	21.47
2	15	14 (above) after implantation	5.22	6.01	7.43
2	16	Glow discharge treated Stellite 21 before implantation	5.00	5.76	7.27
2	17	16 (above) after implantation	4.63	5.87	9.09
2	18	Diamond polished carbon before implantation	7.38	2.04	10.26
2	19	18 (above) after implantation	4.94	4.79	6.19
2	20	Polyurethane based electret before implantation	5.70	4.69	1.98
2	21	20 (above) after implantation	5.01	5.97	10.20
3	22	Poly(γ-methyl *L*-glutamate) PMG–α sheet (a)	5.24	4.06	1.40
3	23	PMG–β sheet (b)	5.36	2.60	1.06
3	24	Mixed PMG α/β sheet (c)	5.20	3.89	1.11
3	25	PMG β sheet modified by chloroform (d)	5.15	3.67	2.36
3	26	PMG β sheet after randomizing treatment (e)	5.04	4.47	1.73
3	27	PMG α sheet on water (f)	5.01	4.39	2.16
3	28	Polyglycine (Nylon 2)	5.28	4.71	1.59
3	29	PMG cast from dichloroacetic acid (DCA)	5.45	3.35	1.39
3	30	Poly(benzyl glutamate)PBG cast from DCA	5.51	2.97	2.72
3	31	PMG cast from chloroform	5.31	3.49	1.50
3	32	PMG swelled in formic acid	5.88	2.42	3.86
3	33	PMG cast from formic acid	5.14	4.74	1.69
4	34	Poly(methacrylic ester) of perfluorinated octanol	3.73	1.20	1.99
4	35	Polypyrrolidone (Nylon 4)	5.32	5.03	3.60
4	36	Glass cover slip flame dried from methanol	5.13	5.69	6.20
4	37	Cellophane sheet	5.46	3.95	2.14
4	38	Dimethyl siloxane (Silastic) sheet	4.25	2.11	4.34
4	39	Polytetrafluorethylene (Teflon) sheet	4.56	1.24	1.91
4	40	Polyethylene sheet	6.26	2.79	10.83
4	41	Nylon sheet	5.31	5.22	3.70
4	42	Poly(vinyl fluoride) (Tedlar) sheet	5.93	2.71	1.97
4	43	Poly(vinyl chloride) sheet	6.62	2.10	5.66
4	44	Poly(ethylene terephthalate) sheet	6.04	3.55	2.22
4	45	Cellulose acetate sheet	5.59	3.92	1.69
4	46	GE Sample 1, unbacked silicone membrane, stock silicone rubber	5.58	2.56	16.14
4	47	GE Sample 1, Side No. 1, reverse of Porous side, 80 to 85% silicone	4.58	1.47	2.97
4	48	GE Sample 2, Side No. 2, porous support side	6.11	2.48	15.22
4	49	GE Sample 2, Side No. 1, polycarbonate copolymer (65% silicone)	5.06	3.32	16.97
4	50	GE Sample 3, Side 2 facing card	5.56	3.09	16.77
4	51	GE Sample 4, Side 1, facing up, Stock MEM-213 (52–55% silicone)	5.39	2.07	9.01
4	52	GE Sample 4, Side 2, facing card	4.07	1.75	9.44
4	53	GE Sample 5, Side 1, facing up, polycarbonate copolymer (25% silicone)	5.80	2.34	13.40
4	54	GE Sample 5, Side 2, facing card	4.79	2.02	5.02
4	55	UC Mylar sheet	6.26	2.36	4.26
4	56	UC Teflon sheet	4.31	1.03	1.99
4	57	UC Sample 9076-53-1H shiny side (mylar cast)	5.60	2.65	7.43
4	58	Same dull side as received (Teflon cast)	5.88	1.86	9.68
4	59	UC Sample 9076-53-1H shiny side, detergent washed	5.84	2.04	5.03
4	60	UC Sample 9076-53-2H, as received, shiny side	5.13	3.35	1.21
4	61	UC Sample 9076-53-2H, as received, dull side	5.37	1.62	4.19
4	62	UC Sample 9076-53-4H, as received, smooth side	5.30	2.95	3.91
4	63	UC Sample 9076-53-4H, as received, dull side	5.78	1.56	6.82
4	64	UC Sample 9076-53-5H, as received, smooth side	5.03	4.20	2.49
4	65	UC Sample 9076-53-5H, as received, dull side	5.26	2.32	2.69
4	66	UC Sample 9076-53-5H shiny side, detergent washed	5.34	3.33	1.51
4	67	UC Sample 9076-53-6H, as received, smooth side	5.01	3.82	2.43
4	68	69 (above), dull side	5.04	1.86	2.73
4	69	UC Sample 9076-53-7H, smooth side	5.30	2.88	3.09
4	70	UC Sample 9076-53-7H, dull side	6.14	1.22	3.88
4	71	UC Sample 9076-53-7H, smooth side, detergent wash	5.83	2.30	1.61
4	72	UC Sample 9076-53-8H, smooth side	5.23	3.04	2.49
4	73	UC Sample 9076-53-8H, dull side	6.38	1.82	10.43
4	74	UC Sample 9076-53-9H, smooth side	5.70	1.85	4.08
4	75	UC Sample 9076-53-9H, dull side	5.72	1.90	7.19

Reference	Surface no. 4	Surface	α (dyne/cm)$^{1/2}$	β (dyne/cm)$^{1/2}$	$\frac{100\delta}{\gamma_{sv}}$
4	76	UC Sample 9076-53-9H, smooth side, detergent wash	5.44	3.07	2.34
4	77	UC Sample 9076-53-10H, smooth side	5.67	2.42	1.32
4	78	UC Sample 9076-53-10H, dull side	5.89	1.61	5.01
4	79	UC Sample 9076-53-11H, smooth side	5.43	2.57	1.17
4	80	UC Sample 9076-53-11H, dull side	5.64	1.25	4.70
4	81	UC Sample 9076-53-11H, smooth side, detergent wash	5.21	3.78	2.46
4	82	UC Sample 9076-53-12H, smooth side	5.74	2.24	2.77
4	83	UC Sample 9076-53-12H, dull side	5.78	1.62	6.44
4	84	UC Sample 9076-53-13H, shiny side	4.95	3.48	2.18
4	85	UC Sample 9076-53-13H, dull side	5.43	1.68	4.58
4	86	UC Sample 9076-53-13H, shiny side, detergent washed	4.99	3.78	1.44
4	87	UC Sample 9076-53-14H, shiny side	4.67	4.64	4.11
4	88	UC Sample 9076-53-14H, dull side	5.25	1.91	4.47
4	89	UC Sample 9076-53-15H, shiny side	5.22	3.44	2.20
4	90	UC Sample 9076-53-15H, dull side	5.87	1.42	3.59
4	91	UC Sample 9076-53-15H, shiny side, detergent washed	4.90	4.11	2.43
4	92	UC Sample 9076-53-16H, shiny side	5.56	2.76	1.77
4	93	UC Sample 9076-53-16H, dull side	5.17	1.49	4.71
4	94	UC Sample 9076-53-17H, shiny side	4.97	3.99	3.61
4	95	UC Sample 9076-53-17H, dull side	5.74	1.74	5.64
4	96	UC Sample 9076-53-17H, smooth side, detergent washed	5.15	3.58	1.86
4	97	UC Sample 9076-53-18H, shiny side	5.54	2.48	3.72
4	98	UC Sample 9076-53-18H, dull side	6.20	1.74	10.34
4	99	UC Sample 9468-15-1, shiny side	5.64	2.04	3.28
4	100	UC Sample 9468-15-1, dull side	5.35	1.27	3.87
4	101	UC Sample 9468-15-1, shiny side, detergent washed	5.48	3.15	7.84
4	102	UC Sample 9468-15-2, shiny side	5.70	2.23	4.35
4	103	UC Sample 9468-15-2, dull side	5.32	2.52	9.28
4	104	UC Sample 9468-15-3, smooth side	5.33	2.32	1.66
4	105	UC Sample 9468-15-3, rough side	5.52	1.74	6.72
4	106	UC Sample 9468-15-3, smooth side, detergent washed	5.31	3.86	5.50
4	107	Parylene AF-4	6;52	1.56	8.22
4	108	Parylene after glow discharge	4.30	6.67	5.82
5	109	UC Sample 9076-53-3H, shiny side	4.99	3.67	2.81
5	110	UC Sample 9076-53-3H, shiny side, detergent washed	5.40	2.85	2.25
5	111	UC Sample 9076-53-3H, dull side	5.20	1.51	2.09
5	112	Nickel ring, glow discharge (*GD*) treated, after 2 h implantation, patent	4.35	6.25	9.98
5	113	Nickel ring, *GD* treated, after 2 h implantation, thrombosed	6.62	2.48	1.09
5	114	Magnesium ring, *GD* treated, after 2 h implantation, patent	4.95	5.13	7.95
5	115	Stellite ring, *GD* treated, stored in distilled water	5.02	6.02	8.15
5	116	Stellite ring, *GD* treated, after 2 h implantation, patent	5.01	5.29	7.47
5	117	Stellite ring, *GD* treated, after 2 week implantation, patent	5.19	5.32	9.35
5	118	Chemically polished copper ring stored 16 h in absolute alcohol	5.35	5.99	8.82
5	119	Copper ring No. 2 thrombosed in 2 h	5.08	5.52	7.42
5	120	Copper ring No. 3 thrombosed in 2 h	4.85	6.09	8.65
5	121	Copper ring No. 4 thrombosed in 2 h	5.83	3.99	2.04
5	122	GDT copper ring No. 5, patent after 2 h	4.79	6.01	9.29
5	123	GDT copper ring No. 2, 2nd acute implant, small junction thrombus	4.96	5.04	3.90
5	124	GDT copper ring No. 4, 2nd acute implant, thrombosed	5.77	3.21	1.77
5	125	GDT aluminium ring No. 2, patent, acute	4.97	3.83	3.15
5	126	GDT aluminium ring No. 3, patent after 2 h	4.70	5.92	5.68
5	127	Aluminium ring No. 4 after chronic implant	5.30	4.05	3.03
5	128	GDT aluminium ring No. 6, patent after 2 weeks	5.05	5.22	6.64
5	129	GDT aluminium ring No. 3, thrombosed in 2 h	5.42	4.83	7.50
5	130	Chemically polished ring No. 4 (aluminium) thrombosed after 2 h	5.67	3.70	1.12
5	131	Chemically polished aluminium ring No. 6 thrombosed at 2 h	5.16	5.67	8.66
5	132	GDT aluminium tube No. 1, patent after 2 h	5.13	3.61	5.56
6	133	Barium Stearate monolayer on GE prism	4.82	1.57	2.36
6	134	Siliconized GE plate, ultrasonic cleaned in acetone	4.59	1.68	1.59
6	135	Siliconized GE plate	4.65	1.27	2.19
6	136	Siliconized GE plate rinsed in seawater and fresh water	4.62	1.26	1.86
6	137	Fibrinogen on GE prism (siliconized), distilled water rinse	4.75	1.82	1.07
6	138	Polycarbonate ring, detergent wash, distilled water rinse	5.58	3.41	1.42
6	139	Ballooned abdominal aorta (rabbit) air dried	5.19	3.38	4.36
6	140	Ballooned right iliac artery (rabbit) air dried	5.36	3.26	1.52
6	141	Left iliac artery (rabbit) air dried	5.29	3.51	3.00
6	142	Fluorinated ethyl cellulose film, air side, detergent washed	4.51	2.22	2.07
6	143	Fluorinated ethyl cellulose film, glass side, detergent washed	4.71	2.34	1.72
6	144	H-span, dehydrated, smooth side, USDA	4.93	5.24	8.07
6	145	H-span, hydrated, smooth side, USDA	5.37	3.67	7.96
6	146	SRI segmented polyether urethane	5.62	2.73	3.64
6	147	SRI polyether urethane	5.58	2.70	3.26
7	148	PAS coated coverslip, as received	4.93	1.93	3.96
7	149	PAS coated coverslip (from AVCO)	5.03	1.76	4.23
7	150	PAS coated coverslip (from AVCO)	4.85	1.66	3.40

Reference	Surface no. 4	Surface	α (dyne/cm)$^{1/2}$	β (dyne/cm)$^{1/2}$	$\frac{100\delta}{\gamma_{sv}}$
7	151	AVCOTHANE balloon, outside surface, as received	4.44	1.36	3.06
7	152	AVCOTHANE balloon, outside surface, after fatigue test	4.48	1.36	3.16
7	153	Polyglycine cast from dichloroacetic acid, distilled water leach	5.38	5.05	2.59
7	154	Poly(*L*-alanine) cast from DCA, as prepared	4.67	7.05	15.38
7	155	Poly(*L*-alanine) film distilled water leached	6.34	2.10	7.16
7	156	Poly(*L*-alanine) film distilled water leached	5.65	3.74	2.48
7	157	Clean teflon plate	4.46	1.33	1.61
7	158	Teflon plate after 5 min contact human plasma	4.74	1.98	1.58
7	159	Fluorinated polyacrylate, Type F film	3.55	1.59	2.36
7	160	Fluorinated polyester Type CT film	3.45	0.95	1.34
7	161	Cell adhesive treated polystyrene	4.99	5.28	3.43
7	162	Polished Stellite 21, 30 sec contact 0.2% fibrinogen	5.68	2.92	2.49
7	163	Polished Stellite 21 plate as received	4.88	1.36	3.47
7	164	Grafted Hydrogel continuously hydrated	5.81	3.86	10.97
7	165	Grafted Hydrogel air dried	5.25	3.44	1.64
7	166	Unalloyed pyrolytic carbon, low temperature isotropic (LTI)	6.48	1.97	6.97
7	167	Carbon coated GE	6.75	2.42	6.65
7	168	Carbon coated prism, 2 min contact with 0.2% fibrinogen	5.88	2.64	3.18
7	169	Carbon coated prism, 30 sec contact 0.2% fibrinogen	5.38	3.51	1.61
7	170	Carbon coated steel, 30 sec contact 0.2% fibrinogen	5.19	3.49	1.60
7	171	Biomer segmented polyether urethane autoclaved	5.19	2.20	2.78
7	172	Dow Corning 236 dispersion coated film	4.82	1.50	3.47
7	173	Ethyl cellulose perfluorobutyrate (PFB) coating, as received	4.14	2.62	6.75
7	174	Ethyl cellulose PFB coating, hydrated	4.35	2.13	1.65
7	175	Air dried side PFB coating exposed to fibrinogen solution	5.08	3.07	2.80
7	176	Hydrated PFB coating exposed to fibrinogen solution	5.55	2.85	2.28
7	177	Sample No. 1, Hydrated acrylomide graft (HAG) on SRI urethane	5.74	2.64	0.85
7	178	Sample No. 3, HAG on SRI polyurethate, fibrinogen exposed	5.73	3.67	5.58
7	179	Sample No. 6, HAG on SRI urethane preirradiated with UV	4.32	6.66	8.76
7	180	Sample No. 7, HAG with 0.25% crosslinker on SRI urethane	5.39	3.95	13.29
7	181	Sample No. 9, HAG with 0.25% crosslinker on SRI urethane, fibrinogen exposed	5.33	1.95	0.95
7	182	Sample No. 12, HAG with 0.25 crosslinker on preirradiated SRI urethane	5.28	4.10	10.11
7	183	Plasma nitrogen–acetylene–water coated slip cover	5.23	3.87	2.11
7	184	Poly(vinyl acetate–2% crotonic acid) 60% ionomer hydrated	5.74	2.35	3.52
7	185	Polyelectrolyte hydrogel after air drying	5.29	3.18	1.11
7	186	Ion beam deposited (IBD) carbon film on GE, fibrinogen exposed	5.80	2.46	2.06
7	187	IBD carbon film on GE prism No. 49	6.08	1.97	4.43
7	188	IBD carbon film on GE prism No. 59	6.36	1.58	7.51
7	189	IBD carbon film on GE prism No. 31	6.14	1.77	6.18
7	190	IBD carbon film on GE prism No. 42	6.19	2.12	6.99

taken as the analogue for the surface properties of blood plasma. This assumption sets forth the proposition that protein molecular segments (phase 1) are competing with the water molecules of blood plasma (phase 2) for bonding sites on the implant surface (phase 3).

The surface energy properties of fibrinogen, vein intima, can be graphically displayed on a surface energy diagram of α *versus* β as shown in *Figure 2.* This diagram also locates the surface tension properties of water (≈blood plasma) and graphically displays the close relation between the vein intima surface properties and those of water. Inserting the appropriate values for α and β into equation (1) for Δ_{ij} = 0 one calculates an interfacial tension γ_{ij} = 12.1 dyne/cm between blood and fibrinogen as compared to a much lower value of γ_{ij} = 1.0 dyne/cm between the vein intima surface and water. The vein surface thus provides a much closer approach to an ideal interface where $\gamma_{ij} = 0$ than does the fibrinogen film.

BIOADHESION AND BIOCOMPATIBILITY

Substantial evidence[1–8] now shows that the first event that follows the exposure of blood to an implant material is the adsorption of plasma borne protein which covers the implant surface. This adsorbed plasma protein film should modify the surface energy of the implant so as to lower its interfacial tension to blood plasma. From equation (1) the specific set of interfacial tensions between the implant (phase 3), blood plasma (phase 2) and adsorbed plasma protein film (phase 1) are started as follows:

$$\gamma_{12} = (\alpha_1 - \alpha_2)^2 + (\beta_1 - \beta_2)^2 \quad (3)$$

$$\gamma_{13} = (\alpha_1 - \alpha_3)^2 + (\beta_1 - \beta_3)^2 \quad (4)$$

$$\gamma_{23} = (\alpha_2 - \alpha_3)^2 + (\beta_2 - \beta_3)^2 \quad (5)$$

For adsorbed plasma protein (phase 1) to spontaneously displace blood plasma (phase 2) from the implant (phase 3) the spreading coefficient S, for phase 1 must be positive. The phase 1 spreading coefficient is defined as:

$$S_1 = \gamma_{23} - \gamma_{13} - \gamma_{12} \quad (6)$$

As shown in equation (6), protein adsorption is favoured by large values of γ_{23}. As shown in equation (5) a large mismatch in implant surface properties α_3, β_3 and blood plasma $\alpha_2 \approx 4.67$, $\beta_2 \approx 7.14$ (dyne/cm)$^{1/2}$ is seen to increase γ_{23}

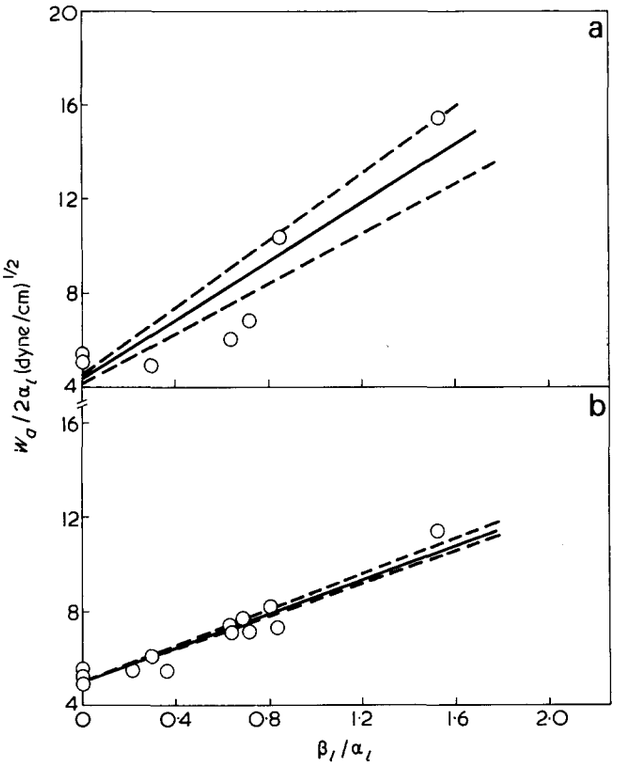

Figure 1 Analytic definition of surface tension properties of (a) vein intimal surface, dog(surface 2 of *Table 4*), γd = 19.5 ± 2.6; γp = 38.2 ± 9.5 dyne cm; α = 4.42; β = 6.18; (b) human fibrinogen thin film (surface 1 of *Table 4*), γd = 2.46 ± 0.7; γp = 13.5 ± 0.9 dyne/cm, α = *4.96;* β = 3.67

and enhance protein adsorption.

The complementary proposition in equation (6) is that minimum values of both γ_{13} and γ_{12} also favour protein adsorption. Equation (3) shows that a minimum mismatch in the surface properties $\alpha_1 \simeq \alpha_2$ and $\beta_1 \simeq \beta_2$ reduces γ_{12}. A similar minimization of γ_{13} is obtained by achieving $\alpha_1 \approx \alpha_3$ and $\beta_1 \approx \beta_{13}$ as shown in equation (4). The present analysis of protein analogues, see surfaces no. 22–23 in *Table 4,* shows that the polar β part of surface energy is substantially varied by solvent–polymer interactions and resultant polymer chain conformation. It is reasonable to presume that plasma protein will be adsorbed on an implant surface with chain conformations which tend to minimize both γ_{12} and γ_{13} by spontaneous adjustment of α_1 and β_1 values in the protein film. By spontaneously minimizing γ_{12} and γ_{13}, the adsorbed plasma protein film evidently performs an important biological adaptation function.

The physiochemical description of the plasma displacement and protein adsorption on the implant surface is analogous to 'priming' as familiarly described in paint technology. Attachment of platelets with formation of thrombus and subsequent thrombus release to produce embolism appears to be mediated by the protein prime layer. Clinical tests of biocompatibility are briefly described in the Appendix by two in vivo tests in common usage. The vena cava test developed by Gott and coworkers[17,19] is limited to the detection of thrombus. The renal embolus test, developed by Kusserow and coworkers[18,19] detects both thrombus and embolism generated by thrombus release from the implant surface. Recent studies by Baier and coworkers[7] now reveal that implant surfaces with evident high thrombo-resistance in the vena cava test are shown to be thrombogenic in the renal embolus test where inspection of the kidney reveals extensive implant damage. The indications are that the thrombus can form on the implant surface and continuously spall off to be carried and deposited in the kidney. The end result is a relatively thrombus free implant surface that acts as a continuous embolus generator. Simple inspection of the implant surfaces at the site of implantation is therefore not a sufficient test for biocompatibility.

A central issue in a revised definition of biocompatibility can be related to the resistance to detachment of the plasma protein film which 'primes' and biologically modifies the implant surface. The modified Griffith relations of *Table 2* provide a quantitative means for evaluating the Griffith energy γ_G required to detach the adsorbed protein film (phase 1) from the implant (phase 3) in the presence of blood plasma (phase 2). The studies summarized in *Table 4* include surface energy analysis of implant materials before and after implantation. Surfaces no. 14–21 studied by Baier and coworkers[2] furnish data for the calculations of the Griffith surface energy γ_G as summarized in *Table 5.*

The calculations in *Table 5* show that the Griffith surface energy γ_G and related critical mechanical stress σ_c decrease as the polar component β_3 of the implant surface increases. The clinical ratings of biocompatibility listed in the lower portion of *Table 5* show a direct correlation between increased γ_G and improved blood compatibility. The results of *Table 5* can be mapped on surface energy diagrams of α *versus* β as shown in *Figure 3. Figure 3b* for polished carbon defines high γ_G with decreasing values of γ_G in clockwise direction to show surface cleaned stellite 21 metal in the lower right view as most highly thrombogenic. The surface energy diagrams of *Figure 3* show the points *H, K* defined in *Table 2* as the origin of the R and R_0 vectors which define the Griffith fracture energy:

$$\gamma_G = R^2 - R_0^2 \tag{7}$$

as defined in *Table 2.* The magnitude of R_0 which subtracts

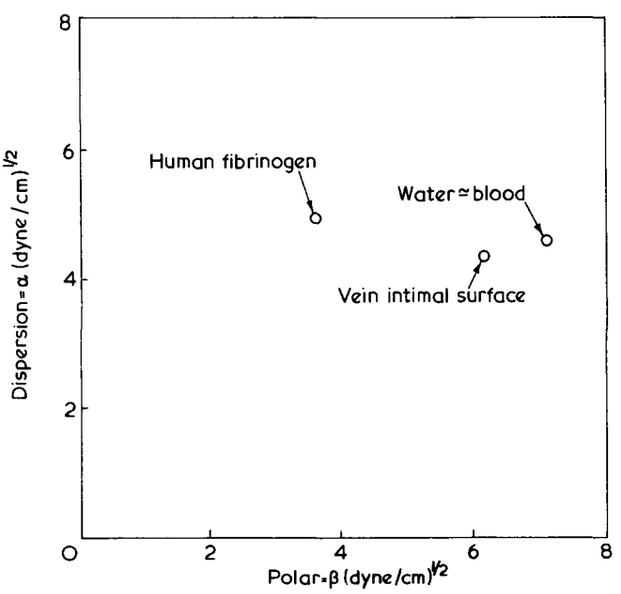

Figure 2 Dispersion (α) and polar (β) surface properties of biological materials

Table 5 Calculated Griffith energy γ_c required to detach adsorbed protein layer (1) from implant surface (3) in blood plasma (2)

Implant	Diamond polished carbon	TDMAC* heparinized silicone	Polyurethane electret	GDT* Stellite 21
Surface no. (see *Table 4*)	18,19	14,15	20,22	16,17
α_3	7.38	5.92	5.70	5.00
β_3	2.04	4.09	4.69	5.76
α_1	4.94	5.22	5.01	4.63
β_1	4.79	6.01	5.97	5.87
α_2	4.67	4.67	4.67	4.67
β_2	7.14	7.14	7.14	7.14
H	6.15	5.57	5.36	4.82
K	3.42	5.01	5.33	5.82
R_0^2	3.38	1.04	0.53	0.04
R^2	16.03	5.35	3.75	1.76
$\gamma_G = (R^2 - R_0^2)$	12.65	4.31	3.70	1.72
Blood compatibility	Excellent[8]	Good[8]	Medium[8]	Poor[7]

* TMDAC = tridodecylammonium chloride; *GDT* = glow discharge treated

from γ_G is related to the mismatch in surface properties between implant (phase 3) and adsorbed protein layer (phase 1). Conversely the manitude of R which adds to γ_G is related to the mismatch between H, K which defines an averaged property of the 1–3 interface and the blood plasma phase. As shown in *Table 5* in all cases the magnitude of R^2 dominantly controls the magnitude of γ_G in the examples graphed in *Figure 3*. The design concept for blood compatibility described by equation (7) incorporates a general argument which details the competition between blood plasma (phase 2) and plasma protein (phase 1) for bonding sites on the implant surface. A high γ_G, indicative of blood compatibility, favours both the spontaneous formation and strong retention of the adsorbed protein film.

DISCUSSION

The previous two sections have briefly introduced and illustrated methods for analysis of surface energy and bioadhesion. The detailed discussion of all relevant aspects of the extensive data compilation in *Table 4* is beyond the scope of this brief report. Review of *Table 4* in conjunction with the extensive experimentation and discussion by Baier and coworkers in the original references[1–7] shows general agreement with the results illustrated here wherein a combination of high dispersion (α) combined with low (β) correlates with high blood compatibility. The previous section relates this result with the strong adsorption and stable retention of a plasma protein adsorption layer on the implant surface.

If the virgin implant surface has a highly polar character which approaches the β values for water or blood plasma the examples show that the protein layer is weakly adsorbed and held on the implant surface. In this later case, the incompletely covered implant would appear to operate efficiently as a thrombus and embolus generator.

This preliminary application of surface energy analysis and the modified Griffith criteria of *Table 1* and *Table 2*, respectively, is quite encouraging. Nyilas and coworkers[10] have reported a series of studies of thrombus formation under closely controlled blood flow conditions. Within a given category of implant materials a high polar property β for the implant surface is shown to correlate with low thromboresistance for a given shear rate of blood flow. This result of Nyilas and coworkers[10] is in agreement with the modified Griffith analysis of critical scress σ_c or energy γ_G for debonding applied in this report.

The adsorption theory outlined in *Table 1* and *Table 2* and applied in this report does not directly treat the effects of either surface roughness or interdiffusion effects related to solvolytic interactions at the interface. Kaelble[12] has developed the thermodynamic extensions of adsorption theory of interfaces to treat both roughness and interdiffusion. The effects of microroughness at the implant surface is potentially a dominant issue in surface energetics at the microfibre scaffold surface used for anchoring viable fibroplastic and endothelial cells to produce a 'living' blood compatible surface.

The adsorption theory is also ill equipped to deal quantitatively with time dependent changes in bioadhesion arising from interdiffusion effects. This latter point is graphically evident in the data scatter shown for blood vessel intima in *Figure 1a*. The natural linings of blood vessels are hydrogels. Synthetic hydrogel coatings consisting of a coherent three dimensional polymer network containing a large proportion of water display promise as implant surfaces[8]. A more detailed description of the role of both *adsorbed* and *absorbed* water on the bioadhesion of hydrogel coatings and biologically deposited protein films require use of a combined adsorption interdiffusion (A-I) theory.

The right column of *Table 4* lists the percent standard deviation from the mean ($100\,\delta\gamma_{sv}^{-1}$) for computed average values of γ_{sv}. Of the 190 surfaces examined, 134 display standard deviations of less than 5% and 175 surfaces give deviations less than 10%. The maximum standard deviation for solid No. 14 is 21.47%. Large standard deviations are generally related to roughness and interdiffusion effects and readily identified in data displays as shown in *Figure 1*. Imprecise values of α and β are, of course, carried forward into the calculations of γ_G as presented in *Table 5*.

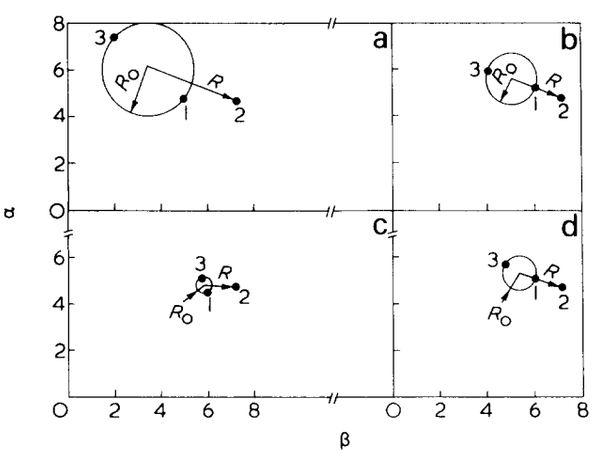

Figure 3 Surface energy analysis of interfacial interactions between plasma protein (phase 1), blood plasma ≈ water (phase 2), and implant (phase 3). (a) 1, 3 (above) after implantation; 2, water ≈ blood plasma; 3, diamond polished carbon. (b) 1, 3 (above) after implantation; 2, water ≈ blood plasma; 3, TDMAC heparanized silicone. (c) 1, 3 (above after implantation; 2, water ≈ blood plasma; 3, GDT Stellite 21. (d) 1, 3 (above) after implantation; 2, water ≈ blood plasma; 3, polyurethane electret

CONCLUSIONS

As a result of this study, some conclusions concerning the role of surface energetics in bioadhesion can be made as follows:

(A) Surface energy analysis is successfully applied to define the dispersion (α) and polar (β) surface energies of 190 biological and implant surfaces.

(B) These dispersion–polar surface energies are introduced into fracture mechanics relations for bioadhesion and biocompatibility.

(C) These fracture mechanics calculations indicate that blood compatibility of an implant is enhanced by spontaneous absorption and strong retention of a plasma protein film on the implant surface.

(D) High dispersion–low polar surface energy for the implant as exemplified by low temperature isotropic (*LTI*) carbon with $\alpha \geqslant 6.0$ (dyne/cm)$^{1/2}$, and $\beta \leqslant 2.0$ (dyne/cm)$^{1/2}$, provide surface energetics favouring stable plasma protein film retention.

(E) Low dispersion–high polar surfaces, typified by surface treated Stellite 21 with $\alpha \approx 5.0$ (dyne/cm)$^{1/2}$, $\beta \geqslant 5.0$ (dyne/cm)$^{1/2}$, provide surface energetics, appear to favour weak adsorption and retention of the plasma protein such that the implant may continuously generate and spall off emboli into the blood stream.

(F) The present analysis can be extended to describe the effects of interface roughness and interdiffusion which represent dominant considerations in microfibre scaffold surfaces, hydrogel coatings, and biological intimal surfaces of the cardiovascular system.

The extensive listing of surface energies in *Table 4* is intended to be used in conjunction with the referenced data sources. The main objective in the discussion is to illustrate, by examples, the usefulness of this surface energy analysis (see *Figure 1*) and the application of the analysis of spontaneous bonding and debonding (see *Figures 2* and *3*).

ACKNOWLEDGEMENTS

The authors wish to gratefully acknowledge the cooperation of L. W. Crane in computations and data analysis. This work was supported under Contract NAS7-100.

REFERENCES

1 Baier, R. E., Dutton, R. C. and Gott, V. L. 'Advances in Experimental Medicine and Biology', (Ed M. Blank), Plenum Press, New York, 1970, Vol 7, pp 235
2 Baier, R. E., Gott, V. L. and Feruse, A. *Trans. Am. Soc. Artif. Int. Organs* 1970, **16**, 50
3 Baier, R. E. and Zisman, W. A. *Macromolecules* 1970, **3**, 70
4 Gott, V. L. and Baier, R. E. PH 43-68-84-4-2 (public document available from the National Technical Information Service, 5285 Port Royal Road, Springfield, Virginia 22151), May 1973
5 Gott, V. L. and Baier, R. E. PH-43-68-84, Volume 2, (public document available from the National Technical Information Service, 5285 Port Royal Road, Springfield, Virginia 22151), September 1973
6 Baier, R. E., dePalma, V. A., Goupil, D., Perlmutter, S., Gott, V. L. and O'Riordan, J. HB-3-2953-1, (public document available from the National Technical Information Service, 5285 Port Royal Road, Springfield, Virginia 22151), February 1975
7 Baier, R. E., Akers, C., Perlmutter, S., Gott, V. L. and O'Riordan, J. CALSPAN Report No. WO6-EB-5307-M-18, prepared for the Biomaterials Program, Division of Heart and Vascular Diseases, National Institute of Health, National Heart and Lung Institute, Bethesda, Maryland 20014, USA, March 1976
8 Bruck, S. D. 'Blood Compatible Synthetic Polymers', Charles C. Thomas, Springfield, 1974
9 Zisman, W. A. 'Adhesion and Cohesion', (Ed. P. Weiss), Elsevier, Amsterdam, 1962, p 176
10 Nyilas, E., Morton, W. A., Cumming, R. D., Lederman, D. M. and Chiu, T-H, *Polym. Prepr.* 1975, **16**, 165
11 Kaeble, D. H. *J. Adhes.* 1970, **2**, 66
12 Kaeble, D. H. 'Physical Chemistry of Adhesion', Wiley–Interscience, New York, 1971, Chs. 5, 13
13 Kaelble, D. H. *SAMPE Q.* 1976, 7, 30
14 Altman, L. P. *Fed. Proc. Fed. Am. Soc. Exp. Biol.* 1961, **20**, 12
15 Dusek, K., Bohdecky, M. and Prokapova, E. *Eur. Polym. J.* 1974, **10**, 239
16 Daelble, D. H. *J. Appl. Polym. Sci.* 1974, **18**, 1869
17 Gott, V. L., Ramos, M. D., Majjar, F. B. and Allen, J. L. *Proc. Artificial Heart Program Conf. 1969*, p 181
18 Kusserow, B., Larrow, R. and Nickols, J. *Fed. Proc. Fed. Am. Soc. Exp. Biol.* 1971, **30**, 1516
19 Bruck, S. D. 'Blood Compatibility Synthetic Polymers', Charles C. Thomas, Springfield, 1974, p 87

APPENDIX

Clinical tests for inplant biocompatibility

Vena cava test. This test was developed by Gott and coworkers[17,19]. Rings (length = 9 mm, and diameters o.d. = 8 mm and i.d. 7 mm) with streamlined edges to prevent turbulence are fabricated from the test material or surface coated with the test material. Implantation is made in the inferior vena cava of a 7.7 to 19.4 dg dog. The rings are inserted with a special device to insure noncontact with the atrial wall or contamination with tissue fluid during implantation.

For *acute* studies (2 h) the chest remains open. At the end of the two hour period the vena cava above and below the ring is doubly clamped and the ring is quickly excised. The inside of the ring is examined within a minute. The extent and nature of the gross thrombus is recorded immediately on a standard ring chart.

For *chronic* studies (2 weeks) the same implantation techniques are used. After implantation, the chest is closed and the animal maintained two weeks before sacrifice. The chest cavity is quickly opened, the ring excised and examined for the extent and nature of thrombus and results recorded on the standard ring chart. In addition, there is a gross inspection of the lungs for any pulmonary pathology and pulmonary embolae.

Renal embolus test. This test was developed by Kusserow and coworkers[18,19]. A ring (length = 10 mm, and diameters o.d. = 8.6 mm and i.d. = 7 mm) is implanted into the abdominal aorta of the test animal immediately above the origin renal arteries. A construction is made in the aorta slightly below the origin of the renal arteries so that over 90% of the blood flowing through the ring must pass through the kidneys. After an implantation period of three to five days an autopsy is performed. The extent of surface thrombus of the ring is assessed by direct visual observation. Embolism is evaluated by direct visual and microscopic examination of both kidneys. The kidneys serve as efficient biological accumulators for the embolic phenomena because the emboli produce recognizable infarcts in these organs.